Revista de Matemática: Teoría y Aplicaciones **32**(1): 15-33
CIMPA - UCR ISSN: 1409-2433(Print), 2215-3373(Online)
DOI: https://doi.org/10.15517/rmta.v32i1.59472

A TWO-LEVEL OVERLAPPING SCHWARZ PRECONDITIONER FOR DISCONTINUOUS GALERKIN METHODS

UN PRECONDICIONADOR DE SCHWARZ DE DOS NIVELES CON TRASLAPE PARA MÉTODOS DISCONTINUOS DE GALERKIN

Juan G. Calvo[1] Moisés Solano[2]

Received: 05/Jun/2024; Accepted: 17/Dic/2024

Revista de Matemática: Teoría y Aplicaciones is licensed under a Creative Commons Reconocimiento-NoComercial-Compartirigual 4.0 International License.
Creado a partir de la obra en http://www.revistas.ucr.ac.cr/index.php/matematica

[1] Universidad de Costa Rica, Centro de Investigación en Matemática Pura y Aplicada, San José, Costa Rica. E-Mail: juan.calvo@ucr.ac.cr
[2] Universidad de Costa Rica, Escuela de Matemática, San José, Costa Rica. E-Mail: moises.solano@ucr.ac.cr

Abstract

This article introduces a two-level overlapping additive Schwarz algorithm tailored for solving elliptic problems discretized with the symmetric interior penalty discontinuous Galerkin method. The proposed algorithm allows for the use of irregular subdomains, overcoming limitations of other approaches where the coarse mesh was based on triangular elements. Additionally, we provide a brief description of the numerical implementation of the Galerkin method. We present numerical results validating the relevance of our algorithm, including cases where the coefficient of the differential equation is discontinuous—a feature that is particularly relevant to various practical applications.

Keywords: domain decomposition; discontinuous Galerkin methods; irregular subdomain boundaries; overlapping Schwarz algorithms; nodal elliptic problems.

Resumen

Este artículo presenta un algoritmo aditivo de Schwarz de dos niveles con traslape diseñado para resolver problemas elípticos discretizados con el método Galerkin discontinuo de penalización interior simétrico. El algoritmo propuesto permite utilizar subdominios irregulares, superando limitaciones de otros enfoques donde la malla gruesa se basaba en elementos triangulares. Se incluye además una breve descripción de la implementación numérica del método de Galerkin. Se presentan resultados numéricos que validan la pertinencia del método, incluyendo casos donde el coeficiente de la ecuación diferencial es discontinuo, una característica que es relevante en diversas aplicaciones.

Palabras clave: descomposición de dominios; métodos discontinuos de Galerkin; subdominios con frontera irregular; algoritmos con traslape de Schwarz; problemas elípticos nodales.

Mathematics Subject Classification: Primary: 65F08, 65F10. Secondary: 65N30, 65N55.

1. Introduction

In this paper we study a preconditioner suitable for linear systems that arise from the discretization of partial differential equations (PDEs) using discontinuous Galerkin methods (DGMs). We focus on Poisson's equation on a given polygonal domain $\Omega \subset \mathbb{R}^2$ with homogeneous Dirichlet boundary conditions:

$$\begin{aligned} -\operatorname{div}(\rho \nabla u) &= f \quad \text{in } \Omega, \\ u &= 0 \quad \text{on } \partial\Omega, \end{aligned} \tag{1}$$

where ρ is a given coefficient. Let $H_0^1(\Omega)$ denote the usual Sobolev space consisting of all functions $u \in L^2(\Omega)$, such that $\nabla u \in (L^2(\Omega))^2$, with vanishing trace. A weak

formulation for problem (1) is posed in $H_0^1(\Omega)$, which is given by: Find $u \in H_0^1(\Omega)$ such that

$$a(u,v) := \int_\Omega \rho \nabla u \cdot \nabla v = \int_\Omega fv =: (f,v)_0 \qquad \forall v \in H_0^1(\Omega), \tag{2}$$

where $\rho \in L^\infty(\Omega)$ is a function such that $\rho(x) \geqslant \alpha > 0$ for some constant α.

We define a finite-dimensional space V_h and a symmetric positive definite bilinear form

$$a_h(\cdot,\cdot) : V_h \times V_h \to \mathbb{R},$$

in order to formulate the discrete problem: Find $u_h \in V_h$ such that

$$a_h(u_h, v_h) = (f, v_h)_0 \quad \forall v_h \in V_h. \tag{3}$$

If $\langle \phi_1, \ldots, \phi_m \rangle$ is a basis of V_h, problem (3) is equivalent to an ill-conditioned linear system of equations of the form $A\boldsymbol{\lambda} = \boldsymbol{b}$, where the matrix $A \in \mathbb{R}^{m\times m}$ has entries $A_{ij} = a_h(\phi_j, \phi_i)$ for $i, j \in \{1, \ldots, m\}$, the vector $\boldsymbol{b} \in \mathbb{R}^m$ has entries $b_j = (f, \phi_j)_0$, and the unknown vector $\boldsymbol{\lambda} \in \mathbb{R}^m$ contains the coordinates of the solution u_h in the basis of V_h; i.e., $u_h = \sum_{j=1}^m \lambda_i \phi_i \in V_h$.

The class of discontinuous Galerkin methods can be traced back to [2], where a fourth-order PDE is solved with piecewise polynomials that are not necessarily continuous. For a comprehensive analysis of these methods and their applications, see [1, 7, 8, 15] and the references therein. DGMs offer advantages such as the use of non-uniform and unstructured meshes, as well as solving time-dependent problems with time discretizations [12]. However, since the total number of degrees of freedom is greater than when using continuous spaces, it is relevant to study preconditioning methods for these linear systems.

Previous studies related to overlapping Schwarz methods for DGMs include [11, 12, 13], where the coarse triangulation is based on triangles. We instead consider general domain decompositions and define an algorithm suitable for irregular partitions, which are relevant for various practical applications. Additionally, we experimentally confirm that our algorithm is effective for piecewise-discontinuous coefficients ρ in (1), as opposed to previous works assuming $\rho(x) = 1$. These studies deduce a bound of the form

$$\kappa \leqslant C\left(1 + \frac{H}{\delta}\right)$$

for the condition number κ of the preconditioned system, where C is independent of the number of subdomains and the size of the elements. The parameter H/δ represents the maximum ratio of the diameter H_i of the subdomain Ω_i and the overlap width δ_i of the corresponding overlapping subdomain Ω_i'; see Section 3.2 for further details. Our algorithm preserves this bound despite using irregular subdomains.

For conforming spaces, discrete harmonic functions were introduced to handle irregular subdomains in [10]. While there are alternative methods to avoid such

expensive construction [3, 4], we consider discrete harmonic extensions for the sake of simplicity; see [16, Chapter 4] for further details. We refer to [3, 4] for a complete study and implementation details on economic variants based on projections over polynomial spaces for the case of continuous spaces.

The remainder of the paper is organized as follows. In Section 2, we briefly describe a DGM for problem (1), focusing solely on a symmetric variant. We then describe the general theory of Schwarz preconditioners and our preconditioner for the discretized problem in Section 3. In Section 4, we include some implementation details for DGMs applied to problem (1). Some numerical experiments that confirm the algorithm's competitiveness are shown in Section 5. We conclude with some final remarks in Section 6.

2. Discontinuous Galerkin method

We briefly describe the lowest-order DGM for nodal elliptic problems in two dimensions for our model problem (1); see [1] for a unified analysis of discontinuous Galerkin methods for elliptic problems, [8, 15] for a complete study, [7] for an interior penalty DGM applied to meshes with arbitrarily-shaped elements, and [5] where our numerical implementation of the method can be downloaded.

For the discretization of (2), let $\{\mathcal{T}_h\}_{h>0}$ be a family of triangulations of Ω with diameter h, composed of general, simple triangular elements. See Section 5 for examples of the meshes considered in our numerical experiments. For an element $E \in \mathcal{T}_h$, denote by $\mathcal{P}_1(E)$ the local space of linear polynomials defined in E. We can choose the degrees of freedom for a function $v \in \mathcal{P}_1(E)$ as its nodal values on the vertices of the polygon E. Globally, the non-conforming DGM space $V_h \not\subset H_0^1(\Omega)$ is defined as

$$V_h := \{v \in L^2(\Omega) : v|_E \in P_1(E) \ \forall E \in \mathcal{T}_h\}. \tag{4}$$

We follow [9, 15]. Denote by $\mathcal{E}_h^i$ and $\mathcal{E}_h^b$ the set of edges of $\mathcal{T}_h$ in the interior and boundary of Ω, respectively, and let $\mathcal{E}_h := \mathcal{E}_h^i \cup \mathcal{E}_h^b$. For each interior edge $e \in \mathcal{E}_h^i$, let E_1^e and E_2^e be the two elements that share e, and $\boldsymbol{n}_e$ the unit normal vector oriented from E_1^e to E_2^e. For a discontinuous function v, we define its average and jump along an interior edge $e \in \mathcal{E}_h^i$ as

$$\{v\}_e := \frac{1}{2}\left(v|_{E_1^e} + v|_{E_2^e}\right), \quad [v]_e := v|_{E_1^e} - v|_{E_2^e},$$

respectively. If $e \in \mathcal{E}_h^b$ is a boundary edge that belongs to the element E_1^e, we simply define

$$\{v\}_e = [v]_e = v|_{E_1^e}.$$

We omit the subscript e when there is no ambiguity.

The weak formulation of problem (1) is given by

$$\sum_{E\in\mathcal{T}_h}\int_E \rho\nabla u\cdot\nabla v - \sum_{e\in\mathcal{E}_h}\int_e \{\rho\nabla u\cdot \boldsymbol{n}_e\}[v] \\ - \sum_{e\in\mathcal{E}_h}\int_e \{\rho\nabla v\cdot \boldsymbol{n}_e\}[u] + \sum_{e\in\mathcal{E}_h}\frac{\sigma_e}{|e|}\int_e [u][v] = \sum_{K\in\mathcal{T}_h}\int_K fv,$$

where $\{\sigma_e\}_e$ are given positive stability constants and $|e|$ is the length of edge e; see, e.g., [9, Section 4.2]. We end up with the symmetric discrete problem: Find $u \in V_h$ such that

$$a_h(u,v) = (f,v)_0 \quad \forall v \in V_h, \tag{5}$$

where

$$a_h(u,v) := a(u,v) - b_1(u,v) - b_1(v,u) + b_2(u,v), \tag{6}$$

and

$$b_1(u,v) := \sum_{e\in\mathcal{E}_h}\int_e \{\rho\nabla u\cdot\boldsymbol{n}_e\}[v], \quad b_2(u,v) := \sum_{e\in\mathcal{E}_h}\frac{\sigma_e}{|e|}\int_e [u][v].$$

For brevity, we omit details regarding the well-posedness of problem (5) and *a priori* estimates; for a comprehensive study, see [8, 9, 15]. It is worth noting that we are considering only the symmetric interior penalty Galerkin variant for simplicity, although other variants of DGM have been widely studied [1].

3. Two-level overlapping Schwarz preconditioner

We describe the standard two-level overlapping Schwarz preconditioner; see [16, Chapter 3] for the abstract Schwarz theory, [16, Chapter 4] for the case of overlapping methods, [3, 4, 10, 17] for specific applications with irregular subdomains, and [6] for a recent study where the coefficient ρ has large variations (referred as a *high-contrast coefficient*).

3.1. Abstract Schwarz theory.

We focus on preconditioning the linear system $A\boldsymbol{\lambda} = \boldsymbol{b}$ that arises from problem (3) with DGMs. Assume there is a family of spaces $\{V_i\}_{i=0}^N$ and interpolation operators $R_i^T : V_i \to V_h$ such that

$$V_h = R_0^T V_0 + \sum_{i=1}^N R_i^T V_i.$$

The space V_0 is called *coarse space*, while the spaces V_i ($i \in \{1,\dots,N\}$) are called *local spaces*. We then introduce symmetric, positive definite bilinear forms on these subspaces,

$$a_i(\cdot,\cdot) : V_i \times V_i \to \mathbb{R}, \ i \in \{0,\dots,N\}.$$

For simplicity, we choose

$$a_i(u_i, v_i) := a_h(R_i^T u_i, R_i^T v_i), u_i, v_i \in V_i;$$

this choice is referred to as *exact solvers*. In this case, the local stiffness matrix $A_i : V_i \to V_i$ associated to $a_i(\cdot,\cdot)$ is given by $A_i = R_i A R_i^T$, where $R_i = (R_i^T)^T$. Schwarz operators are defined as

$$P_i := R_i^T A_i^{-1} R_i A, \quad i \in \{0, 1, \ldots, N\},$$

and the two-level additive Schwarz preconditioner is defined as

$$P_{ad} := \sum_{i=0}^{N} P_i.$$

The associated preconditioned linear system can be written as

$$P_{ad} u = A_{ad}^{-1} A u = A_{ad}^{-1} b,$$

with

$$A_{ad}^{-1} := \sum_{i=0}^{N} R_i^T A_i^{-1} R_i = \sum_{i=0}^{N} R_i^T (R_i A R_i^T)^{-1} R_i. \tag{7}$$

We remark that the preconditioner A_{ad}^{-1} is determined once we define the operators R_i^T. For the local spaces, defining these operators is straightforward; however, for the coarse space, extra work is usually required when irregular subdomains are present. We describe such constructions in the following sections.

3.2. Local spaces.

We partition the domain Ω into N non-overlapping disjoint subdomains $\{\Omega_i\}_{i=1}^N$ with respective diameters H_i which are the union of elements of $\mathcal{T}_h$. The partition $\{\Omega_i\}$ is called *coarse mesh* and is denoted by $\mathcal{T}_H$. We then construct overlapping subdomains $\Omega_i' \supset \Omega_i$ by adding layers of elements that are external to Ω_i, and we denote by δ_i the maximum width of the region $\Omega_i' \backslash \Omega_i$; see Figure 1 for an example of an irregular decomposition obtained using the graph-partitioner software METIS [14].

We consider the DGM space on each subdomain Ω_i'; i.e., we set

$$V_i := \{v \in L^2(\Omega_i') : v|_E \in P_1(E)\ \forall E \in \Omega_i',\ v|_e = 0\ \forall e \in \partial\Omega_i'\}$$

for each $i \in \{1, \ldots, N\}$. Thus, the extension operators $R_i^T : V_i \to V_h$ can be defined as the zero-extension operators. The matrix A_i associated to the bilinear form $a_i(\cdot,\cdot)$ then corresponds to the sub-block of the stiffness matrix A that includes the degrees of freedom in the interior of Ω_i'. The matrices A_i are positive-definite, and in every step of the iterative method a linear system involving A_i must be solved for each overlapping subdomain. We use the Cholesky factorization, which is computed once and then stored for the remainder of each simulation.

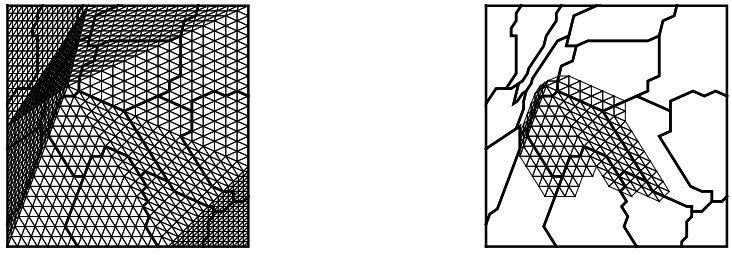

Figure 1: (Left) A domain decomposition with irregular subdomains (black thick lines). (Right) Coarse mesh $\mathcal{T}_H$ (black thick lines) and an overlapping subdomain Ω_j' (small triangles) obtained by adding two layers of elements of $\mathcal{T}_h$.

Remark 1. *A one-level additive preconditioned operator can be defined by*

$$P_{ad,1} := \sum_{i=1}^{N} P_i = A_{ad}^{-1} A, \text{ with } A_{ad}^{-1} = \sum_{i=1}^{N} R_i^T A_i^{-1} R_i.$$

Nevertheless, this preconditioner is not scalable (the condition number of the preconditioned system grows with N); see, e.g., [16, Section 3]. This observation justifies the necessity of a second level, built usually on the coarse mesh $\mathcal{T}_H$.

3.3. Coarse space and extension operator.

As noted in Remark 1, the preconditioner requires a coarse space V_0 in order to obtain a bound for the condition number of the preconditioned system that is independent of the number of subdomains N. Its dimension has to be small enough (since every iteration requires solving a linear system with the matrix A_0), but large enough such that it includes enough information among all subdomains. We focus in the case of irregular subdomains as introduced in [10].

Consider the coarse mesh $\mathcal{T}_H$ with elements $\{\Omega_i\}_{i=1}^N$. The set of *subdomain edges* is defined by

$$\mathcal{S}_\mathcal{E} := \left\{\mathcal{E}^{ij}, 1 \leqslant i < j \leqslant N\right\},$$

where $\mathcal{E}^{ij}$ is the interior of $\overline{\Omega}_i \cap \overline{\Omega}_j$ (common open edge of subdomains i and j). If this intersection has more than one component, each one component will be regarded as an edge of Ω_i. We then define the set of *subdomain vertices*, denoted by $\mathcal{S}_\mathcal{V}$, that contains the endpoints of the subdomain edges that lie inside Ω; see Figure 2.

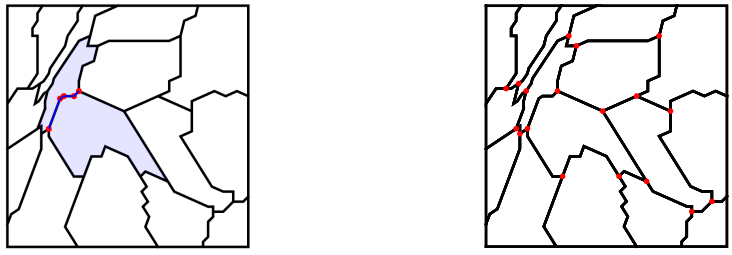

Figure 2: (Left) Two (colored) subdomains, the associated subdomain edge (blue) and its nodes on the coarse mesh (red). (Right) Subdomains and set of subdomain vertices (red). Each polygon on the coarse mesh has an average of 15 vertices. There are 108 vertices in $\mathcal{T}_H$ and 18 subdomain vertices.

A natural initial choice for V_0 is the DGM space (4) defined in $\mathcal{T}_H$ if triangular subdomains are considered, as studied in [13]. We can consider the continuous space of discrete harmonic functions defined in $\mathcal{T}_H$; however, its dimension can be quite large in the presence of irregular subdomains. Instead, we construct one basis function per subdomain vertex and V_0 is defined as the span of such functions. For instance, Figure 2 shows only 17 subdomain vertices, compared to 108 nodes in the polygonal coarse mesh. We restrict ourselves to continuous coarse functions in order to further reduce the dimension of V_0, but discontinuous functions can be considered as well.

Given a subdomain vertex $\boldsymbol{x}_0 \in \mathcal{S}_\mathcal{V}$, we define the values of a coarse function $\psi^H_{\boldsymbol{x}_0}$ on every subdomain edge as follows. First, we set $\psi^H_{\boldsymbol{x}_0}(\boldsymbol{x}) = 0$ for all subdomain vertices $\boldsymbol{x}$, except at $\boldsymbol{x}_0$ where $\psi^H_{\boldsymbol{x}_0}(\boldsymbol{x}_0) = 1$. Second, we define the values of $\psi^H_{\boldsymbol{x}_0}$ on the subdomain edges. If $\boldsymbol{x}_0$ is not an endpoint of $\mathcal{E}$, then $\psi^H_{\boldsymbol{x}_0}$ vanishes on that edge. If $\mathcal{E}$ has endpoints $\boldsymbol{x}_0$ and $\boldsymbol{x}_1$, let $\boldsymbol{d}_\mathcal{E}$ be the unit vector with direction from $\boldsymbol{x}_1$ to $\boldsymbol{x}_0$. Consider any node $\tilde{\boldsymbol{x}} \in \mathcal{E}$. If $0 \leqslant (\tilde{\boldsymbol{x}} - \boldsymbol{x}_1) \cdot \boldsymbol{d}_\mathcal{E} \leqslant |\boldsymbol{x}_0 - \boldsymbol{x}_1|$, we then set

$$\psi^H_{\boldsymbol{x}_0}(\tilde{\boldsymbol{x}}) = \frac{(\tilde{\boldsymbol{x}} - \boldsymbol{x}_1) \cdot \boldsymbol{d}_\mathcal{E}}{|\boldsymbol{x}_0 - \boldsymbol{x}_1|};$$

see [3]. It holds that $\psi^H_{\boldsymbol{x}_0}(\boldsymbol{x}_0) = 1$, $\psi^H_{\boldsymbol{x}_0}(\boldsymbol{x}_1) = 0$ and that the function varies linearly in the direction of $\boldsymbol{d}_\mathcal{E}$ for such nodes. If $(\tilde{\boldsymbol{x}} - \boldsymbol{x}_1) \cdot \boldsymbol{d}_\mathcal{E} < 0$ or $(\tilde{\boldsymbol{x}} - \boldsymbol{x}_1) \cdot \boldsymbol{d}_\mathcal{E} > |\boldsymbol{x}_0 - \boldsymbol{x}_1|$, we then set $\psi^H_{\boldsymbol{x}_0}(\tilde{\boldsymbol{x}}) = 0$ or $\psi^H_{\boldsymbol{x}_0}(\tilde{\boldsymbol{x}}) = 1$, respectively. Finally, for $\boldsymbol{x} \in \Omega_i$, we construct the discrete harmonic extension of the previously defined boundary values.

For completeness, we recall that a function $u^{(i)}$ defined on Ω_i is said to be discrete harmonic on Ω_i if

$$A^{(i)}_{II} u^{(i)}_I + A^{(i)}_{I\Gamma} u^{(i)}_\Gamma = 0,$$

where $A_{II}^{(i)}$ and $A_{I\Gamma}^{(i)}$ are the standard notation for the subblocks of the stiffness matrix $A^{(i)}$ associated to subdomain Ω_i corresponding to the interior degrees of freedom I and boundary degrees of freedom Γ; see, e.g., [16, Section 4.4]. Similarly, $u_I^{(i)}$ and $u_\Gamma^{(i)}$ represent the blocks of $u^{(i)}$ corresponding to the interior and boundary degrees of freedom. It is clear that the interior values $u_I^{(i)}$ are defined uniquely by its values on the boundary $u_\Gamma^{(i)}$.

We then define the coarse space V_0 as

$$V_0 = \operatorname{span}\langle \psi_{\boldsymbol{x}_0}^H \rangle_{\boldsymbol{x}_0 \in \mathcal{S}_\mathcal{V}}.$$

A function $\psi \in V_0$ is uniquely defined by its nodal values on the subdomain vertices, and therefore

$$\dim V_0 = |\mathcal{S}_\mathcal{V}|\,.$$

The interpolation operator $R_0^T : V_0 \to V_h$ has to *approximate* functions in V_0 by functions defined on V_h. In typical studies, such as [13], subdomains are assumed to be regular (triangles or squares in two dimensions), and it is straightforward to interpolate a linear or bilinear function from the coarse to the fine mesh; i.e., R_0^T is the evaluation of the coarse linear/bilinear function on the fine nodes. When irregular subdomains are considered, this is not usually possible. We consider discrete harmonic extensions for simplicity; see [16, Chapter 4] for further details, even though it is possible to define R_0^T as studied in [3, 4].

We remark that for each subdomain vertex $\boldsymbol{x}_0$ we require to solve a linear system on the subdomains that have $\boldsymbol{x}_0$ as a vertex. In Figure 3 we show the degrees of freedom of a coarse function $\psi_{\boldsymbol{x}_0{}^H}$ and its extension $R_0^T \psi_{\boldsymbol{x}_0{}^H}$. The columns of the matrix R_0^T include the values of $R_0^T \psi_{\boldsymbol{x}_0{}^H}$ on the nodes of $\mathcal{T}_h$; see [16, Section 3.7].

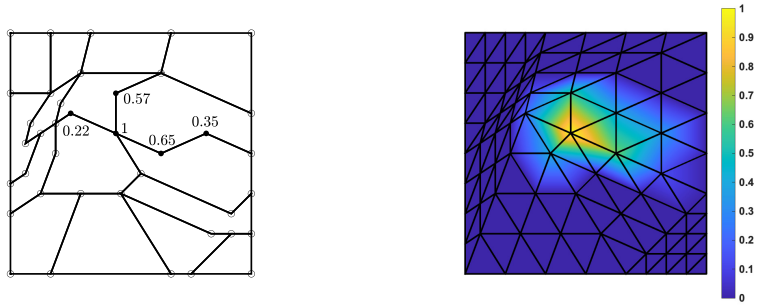

Figure 3: (Left) Degrees of freedom of a function $\psi_{\boldsymbol{x}_0{}^H} \in V_0$; empty circles correspond to nodal values equal to zero. (Right) Extension $R_0^T \psi_{\boldsymbol{x}_0{}^H} \in V_h$ computed as a discrete harmonic extension inside the subdomains.

4. Implementation details

In this section we summarize how the local matrices are computed in order to assemble the stiffness matrix A. These `MATLAB` routines are available to download from [5]. We separate the details for each component of the bilinear form (6), and provide explicit formulas for the local matrices. We also include a brief description of the preconditioner construction.

4.1. Integral over elements.

For a triangle E with vertices $\boldsymbol{v}_1, \boldsymbol{v}_2, \boldsymbol{v}_3$ and associated local basis functions ϕ_1, ϕ_2, ϕ_3, it is known that the local matrix associated to the term

$$\int_E \nabla\phi_i \cdot \nabla\phi_j, \quad i, j \in \{1, 2, 3\},$$

can be written exactly as

$$A_1^{loc} = \frac{1}{4|E|} \begin{pmatrix} \boldsymbol{y}'\boldsymbol{y} & \boldsymbol{y}'\boldsymbol{z} & \boldsymbol{y}'\boldsymbol{x} \\ \boldsymbol{z}'\boldsymbol{y} & \boldsymbol{z}'\boldsymbol{z} & \boldsymbol{z}'\boldsymbol{x} \\ \boldsymbol{x}'\boldsymbol{y} & \boldsymbol{x}'\boldsymbol{z} & \boldsymbol{x}'\boldsymbol{x} \end{pmatrix}, \tag{8}$$

where $\boldsymbol{x} = \boldsymbol{v}_2 - \boldsymbol{v}_1$, $\boldsymbol{y} = \boldsymbol{v}_3 - \boldsymbol{v}_2$, $\boldsymbol{z} = \boldsymbol{v}_1 - \boldsymbol{v}_3$. Equation (8) follows from straightforward computations, given that ϕ_i, ϕ_j are linear functions with $\phi_i(\boldsymbol{x}_k) = \delta_{ik}$, $\phi_j(\boldsymbol{x}_k) = \delta_{jk}$ ($k \in \{1, 2, 3\}$). In the case of $a(\phi_i, \phi_j)$, the contribution of an element E is given by the integral

$$\int_E \rho \nabla\phi_i \cdot \nabla\phi_j = \nabla\phi_i \cdot \nabla\phi_j \int_E \rho,$$

and we use a one-point quadrature rule to approximate $\int_E \rho \approx \rho(\boldsymbol{x}_b^E)|E|$, where $\boldsymbol{x}_b^E$ is the barycenter of E. Therefore, the matrix A_1^{loc} given in (8) has to be multiplied by $\rho(\boldsymbol{x}_b^E)$.

4.2. Integrals over edges.

Consider now the integrals over the edges of the bilinear form. Given an edge e shared by elements E_1^e and E_2^e, let $\boldsymbol{v}_1$, $\boldsymbol{v}_2$ be the endpoints of e, and $\boldsymbol{v}_3^+, \boldsymbol{v}_3^-$ the third vertex of E_1^e and E_2^e, respectively. See Figure 4, which also illustrates the local ordering for the degrees of freedom. Define the vectors $\boldsymbol{x} = \boldsymbol{v}_2 - \boldsymbol{v}_1, \boldsymbol{y} = \boldsymbol{v}_3^+ - \boldsymbol{v}_2, \boldsymbol{z} = \boldsymbol{v}_1 - \boldsymbol{v}_3^+, \boldsymbol{a} = \boldsymbol{v}_3^- - \boldsymbol{v}_2, \boldsymbol{b} = \boldsymbol{v}_1 - \boldsymbol{v}_3^-$.

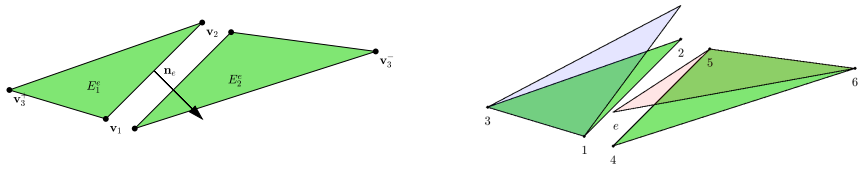

Figure 4: (Left) An internal edge shared by triangles E_1^e and E_2^e, with vertices $\boldsymbol{v}_1, \boldsymbol{v}_2, \boldsymbol{v}_3^+$ and $\boldsymbol{v}_1, \boldsymbol{v}_2, \boldsymbol{v}_3^-$, respectively. (Right) Local index for degrees of freedom and two local basis functions ϕ_2, ϕ_4.

For the bilinear form $b_1(\cdot,\cdot)$, we need to compute

$$\frac{1}{2}\int_e ((\rho\nabla\phi_i)|_{E_1^e} + (\rho\nabla\phi_i)|_{E_2^e}) \cdot \boldsymbol{n}_e(\phi_j|_{E_1^e} - \phi_j|_{E_2^e})$$

for any internal edge e. Since $\nabla\phi_i$ is constant on each element, terms of the form $\int_e \rho\phi_j$ are approximated with a one-point quadrature using the midpoint of e. Define

$$M = \begin{pmatrix} \frac{\boldsymbol{y}\cdot\boldsymbol{x}}{\boldsymbol{y}^\perp\cdot\boldsymbol{x}} & \frac{\boldsymbol{y}\cdot\boldsymbol{x}}{\boldsymbol{y}^\perp\cdot\boldsymbol{x}} & 0 \\ \frac{\boldsymbol{x}\cdot\boldsymbol{z}}{\boldsymbol{x}^\perp\cdot\boldsymbol{z}} & \frac{\boldsymbol{x}\cdot\boldsymbol{z}}{\boldsymbol{x}^\perp\cdot\boldsymbol{z}} & 0 \\ \frac{\boldsymbol{x}^\perp\cdot\boldsymbol{x}}{\boldsymbol{y}^\perp\cdot\boldsymbol{x}} & \frac{\boldsymbol{x}^\perp\cdot\boldsymbol{x}}{\boldsymbol{y}^\perp\cdot\boldsymbol{x}} & 0 \end{pmatrix}, \quad N = \begin{pmatrix} \frac{\boldsymbol{x}\cdot\boldsymbol{a}}{\boldsymbol{x}^\perp\cdot\boldsymbol{a}} & \frac{\boldsymbol{x}\cdot\boldsymbol{a}}{\boldsymbol{x}^\perp\cdot\boldsymbol{a}} & 0 \\ \frac{\boldsymbol{b}\cdot\boldsymbol{x}}{\boldsymbol{b}^\perp\cdot\boldsymbol{x}} & \frac{\boldsymbol{b}\cdot\boldsymbol{x}}{\boldsymbol{b}^\perp\cdot\boldsymbol{x}} & 0 \\ \frac{\boldsymbol{x}\cdot\boldsymbol{a}}{\boldsymbol{x}^\perp\cdot\boldsymbol{a}} & \frac{\boldsymbol{x}\cdot\boldsymbol{a}}{\boldsymbol{x}^\perp\cdot\boldsymbol{a}} & 0 \end{pmatrix},$$

where $\boldsymbol{v}^\perp := (-v_2, v_1)$ for any vector $\boldsymbol{v} = (v_1, v_2)$. The local matrix associated to the bilinear form $b_1(\cdot,\cdot)$ for the edge e can be approximated in block form as

$$B_{e,1}^{loc} = \frac{1}{4}\begin{bmatrix} \rho^+ M & -\rho^+ M \\ -\rho^- N & \rho^- N \end{bmatrix},$$

where $\rho^+ = \rho|_{E_1^e}$, $\rho^- = \rho|_{E_2^e}$ are the evaluations of ρ at the midpoint of e.

For the last bilinear form $b_2(\cdot,\cdot)$, we need to compute

$$\frac{\sigma_e}{|e|}\int_e (\phi_i|_{K^+} - \phi_i|_{K^-}) \cdot (\phi_j|_{K^+} - \phi_j|_{K^-})$$

for any interior edge e. The associated local matrix for an interior edge e can be computed exactly as

$$B_{e,2}^{loc} = \frac{\sigma_e}{6}\begin{bmatrix} 2 & 1 & 0 & -2 & -1 & 0 \\ 1 & 2 & 0 & -1 & -2 & 0 \\ 0 & 0 & 0 & 0 & 0 & 0 \\ -2 & -1 & 0 & 2 & 1 & 0 \\ -1 & -2 & 0 & 1 & 2 & 0 \\ 0 & 0 & 0 & 0 & 0 & 0 \end{bmatrix}.$$

4.3. Assembling the local matrices.

Once the local edge matrices $B_{e,1}^{loc}$ and $B_{e,2}^{loc}$ have been assembled, we require a local to global mapping of degrees of freedom. For an internal edge, according to the local ordering shown in Figure 4, if elements E_1^e and E_2^e have global degrees of freedom $[v_1, v_2, v_3]$ and $[v_4, v_5, v_6]$, then the entries of $B_{e,1}^{loc}$ and $B_{e,2}^{loc}$ must be added to the entries given by the matrices

$$i_x = \begin{bmatrix} v_1 & v_1 & v_1 & v_1 & v_1 & v_1 \\ v_2 & v_2 & v_2 & v_2 & v_2 & v_2 \\ v_3 & v_3 & v_3 & v_3 & v_3 & v_3 \\ v_4 & v_4 & v_4 & v_4 & v_4 & v_4 \\ v_5 & v_5 & v_5 & v_5 & v_5 & v_5 \\ v_6 & v_6 & v_6 & v_6 & v_6 & v_6 \end{bmatrix}, \quad i_y = \begin{bmatrix} v_1 & v_2 & v_3 & v_4 & v_5 & v_6 \\ v_1 & v_2 & v_3 & v_4 & v_5 & v_6 \\ v_1 & v_2 & v_3 & v_4 & v_5 & v_6 \\ v_1 & v_2 & v_3 & v_4 & v_5 & v_6 \\ v_1 & v_2 & v_3 & v_4 & v_5 & v_6 \\ v_1 & v_2 & v_3 & v_4 & v_5 & v_6 \end{bmatrix},$$

which can be easily obtained with the command `meshgrid`. Similarly, the 3×3 matrices associated to boundary edges are assembled. The local matrix A_1^{loc} is easily assembled according to the degrees of freedom of each triangle.

If A_1, B_1, B_2 denote the global matrices obtained by assembling the local matrices $A_1^{loc}, B_{e,1}^{loc}, B_{e,2}^{loc}$, respectively, then the global stiffness matrix A is given by

$$A = A_1 - B_1 - B_1^T + B_2.$$

4.4. Preconditioner.

Once the stiffness matrix A is assembled, the action of the additive preconditioner (7) can be easily computed by defining the operators R_i^T as follows:

1. For $i \in \{1, \ldots, N\}$, matrices R_i^T map a vector of degrees of freedom in V_i (nodal values in the interior of Ω_i') to its zero extension in V_h. Hence, the j-th column ($j \in \{1, \ldots, N\}$) of R_i^T is a vector with entries equal to 1 if the associated node lies in the interior of Ω_i', and 0 otherwise. It is not necessary to construct explicitly these matrices, since we only require the indices of the interior nodes of each overlapping subdomain.

2. For R_0^T, it is well-known that the j-th column ($j \in \{1, \ldots, |\mathcal{S}_\mathcal{V}|\}$) of R_0^T has the value of the coarse function ψ related to subdomain vertex j evaluated at the fine mesh; for the consicion we omit details and refer to [16, Section 3.7].

5. Numerical results

We present a first experiment that explores the convergence of DGMs; we then test our preconditioner (7) for problem (5) with regular (squares) and irregular (METIS) subdomains [14], with $\rho = 1$ and ρ discontinuous on $\mathcal{T}_h$.

5.1. Convergence of DGM.

For completeness, we first confirm the convergence of our DGM implementation for structured and unstructured triangular meshes as shown in Figure 5. We use $\rho(x_1, x_2) = 1$ and $\rho(x_1, x_2) = x_1x_2 + 1$ for the exact solution $u(x_1, x_2) = \sin(\pi x_1)\sin(\pi x_2)$, with $\sigma_e = 10$ and $\sigma_e = 20$, respectively. We confirm convergence of order h^2 as shown in Figure 6.

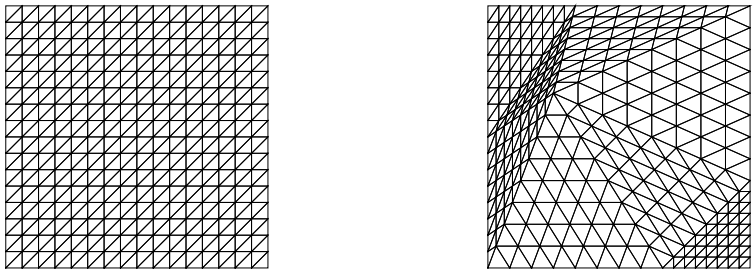

Figure 5: (Left) Structured and (Right) unstructured triangular mesh.

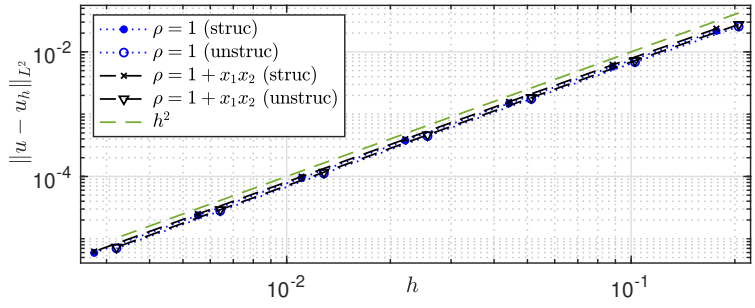

Figure 6: L^2-error as a function of h for DGM, for a structured and unstructured triangular mesh as shown in Figure 5, for $\rho(x_1, x_2) = 1$ and $\rho(x_1, x_2) = 1 + x_1x_2$.

5.2. Preconditioner with constant coefficient.

In this section, we present numerical experiments for preconditioner (7) applied to the linear system obtained using a DGM with $\rho = 1$ for structured meshes. We use $\sigma_e = 10$ and solve the resulting linear systems using the preconditioned conjugate gradient (PCG) method to a relative residual tolerance of 10^{-6}. For each simulation, we report the number of iterations (I), an approximation for the condition number of the preconditioned system (κ) and the dimension of the

coarse space ($\dim V_0$). We recall that authors in [13] obtained similar results for preconditioning DGM discretizations with triangular subdomains only for $\rho = 1$.

First, Table 1 illustrates the dependency on the condition number as we increase the number of subdomains (scalability). The results indicate that the condition numbers and the PCG iterations remain bounded as the number of square and irregular subdomains increases. Second, Table 2 shows that the method does not depend on H/h. Finally, Figure 7 confirms the linear growth of the condition number as a function of H/δ.

Table 1: Condition number (κ) for the preconditioned system $A_{ad}^{-1}A$ and number of PGC iterations (I) as a function of the number of square and irregular subdomains N; $\dim V_0$ is the coarse space dimension and $H/h = 16$. The case $H/\delta = 16$ corresponds to the minimal overlap case $\delta = h$.

H/δ	N	Square subdomains		METIS subdomains	
		I (κ)	$\dim V_0$	I (κ)	$\dim V_0$
16	8^2	20 (14.9)	49	37 (20.3)	97
	12^2	20 (14.1)	121	40 (25.0)	243
	16^2	20 (13.5)	225	40 (24.7)	447
	20^2	18 (13.8)	361	48 (38.6)	711
	24^2	17 (13.9)	529	43 (27.6)	1054
	28^2	17 (14.1)	729	45 (29.6)	1456
	32^2	17 (14.1)	961	48 (35.8)	1915
4	8^2	15 (6.2)	49	25 (9.3)	97
	12^2	14 (6.0)	121	26 (9.8)	243
	16^2	14 (5.8)	225	26 (11.0)	447
	20^2	14 (5.7)	361	29 (13.2)	711
	24^2	14 (5.7)	529	27 (10.3)	1054
	28^2	14 (5.7)	729	29 (11.9)	1456
	32^2	14 (5.7)	961	31 (15.0)	1915

Table 2: Condition number (κ) for the preconditioned system $A_{ad}^{-1}A$ and number of PCG iterations (I) as a function of H/h for square and irregular subdomains, $N = 36$, $H/\delta = 4$ and $\rho = 1$; $\dim V_0$ is the coarse space dimension.

H/h	Square subdomains		METIS subdomains	
	$I(\kappa)$	$\dim V_0$	$I(\kappa)$	$\dim V_0$
8	15 (5.3)	25	24 (10.9)	48
16	15 (5.8)	25	25 (10.8)	48
32	16 (6.3)	25	25 (10.8)	48
64	17 (6.4)	25	26 (10.7)	48

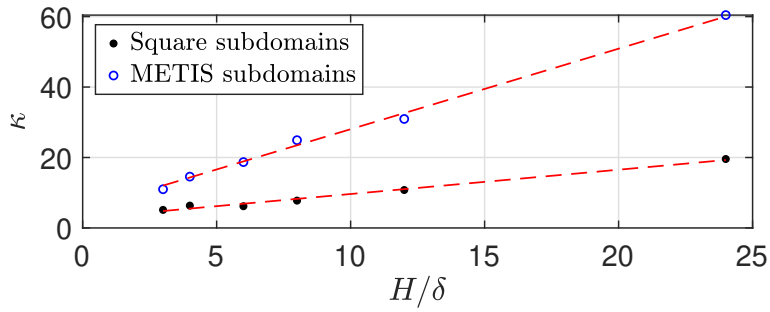

Figure 7: Condition number κ as a function of H/δ for $N = 64$, $H/h = 24$ and $\rho = 1$, for square and METIS subdomains. The dashed red lines represent the best linear fits for the data, with approximate slopes of 0.69 and 2.29, respectively.

5.3. Preconditioner with variable coefficients.

We now present numerical results for two different choices of $\rho(x)$ shown in Figure 8: (i) a piecewise constant ρ on each subdomain, and (ii) a channel distribution where $\rho = 10^3$ for the red channels, and $\rho = 1$ in the background (called in literature as a high-contrast multiscale coefficient). We confirm scalability and study dependence on H/h and H/δ in Table 3, Table 4 and Figure 9 for the case of a random piecewise constant coefficient ρ. We use $\sigma_e = 10^4$.

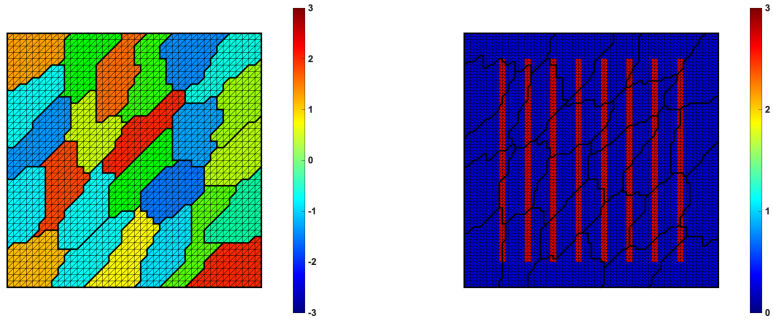

Figure 8: Coefficient ρ for two experiments: (Left) ρ is constant inside each subdomain varying from 10^{-3} (blue) to 10^3 (red). (Right) $\rho = 10^3$ in the red channels and $\rho = 1$ otherwise.

Table 3: Condition number (κ) for the preconditioned system $A_{ad}^{-1}A$ and number of PGC iterations (I) as a function of the number of square and irregular subdomains N; $\dim V_0$ is the coarse space dimension, $H/h = 16$, $H/\delta = 4$ and ρ is piecewise constant as in Figure 8.

N	Square subdomains		METIS subdomains	
	$I(\kappa)$	$\dim V_0$	$I(\kappa)$	$\dim V_0$
8^2	24 (8.7)	49	29 (10.5)	97
12^2	28 (10.8)	121	26 (8.6)	243
16^2	32 (12.1)	225	28 (8.9)	447
20^2	32 (12.4)	361	31 (11.3)	711
24^2	33 (12.5)	529	33 (12.4)	1054
28^2	32 (12.4)	729	35 (13.0)	1456
32^2	32 (12.4)	961	33 (13.2)	1915

Table 4: Condition number (κ) for the preconditioned system $A_{ad}^{-1}A$ and number of PCG iterations (I) as a function of H/h for square and irregular subdomains, $N = 36$ and $H/\delta = 4$; $\dim V_0$ is the coarse space dimension. We use a piecewise constant coefficient ρ as shown in Figure 8.

H/h	Square subdomains		METIS subdomains	
	I (κ)	$\dim V_0$	I (κ)	$\dim V_0$
8	22 (6.8)	25	29 (11.0)	48
16	22 (7.0)	25	26 (11.6)	48
32	22 (6.7)	25	27 (11.2)	48
64	24 (8.4)	25	29 (11.0)	48

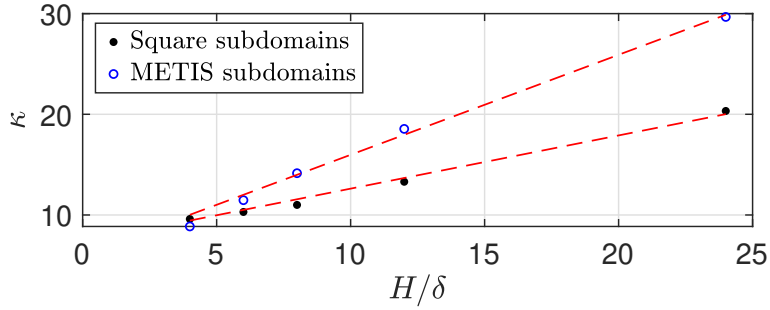

Figure 9: Condition number κ as a function of H/δ for $N = 64$ and $H/h = 24$, for square and METIS subdomains. We use a piecewise constant coefficient ρ as shown in Figure 8. The dashed red lines represent the best linear fits for the data, with approximate slopes of 0.53 and 0.99, respectively.

It is known that the performance of iterative methods depends on the contrast $\eta = \max \rho(x)/\min \rho(x)$. Therefore, competitive results are not expected for the

high-contrast channels shown in Figure 8. As observed in Table 5, the method deteriorates as the number of subdomains increases, with some favourable cases when METIS subdomains are used. However, in general we obtain that κ is of order η. We refer to [6] for a recent work on continuous two-level overlapping methods and references therein for a detailed explanation on previous work for the case of high-contrast coefficients, which can be used for DGMs.

Table 5: Condition number (κ) for the preconditioned system $A_{ad}^{-1}A$ and number of PGC iterations (I) as a function of the number of square and irregular subdomains N; $\dim V_0$ is the coarse space dimension, $H/h = 16$, $H/\delta = 4$ and ρ has a channel distribution as in Figure 8.

N	Square subdomains		METIS subdomains	
	$I(\kappa)$	$\dim V_0$	$I(\kappa)$	$\dim V_0$
64	51 (220)	49	79 (243)	97
144	53 (221)	121	66 (204)	243
256	52 (179)	225	41 (19.6)	447
400	65 (214)	361	39 (16.8)	711

6. Conclusions and final remarks

We have presented a two-level overlapping Schwarz preconditioner for discontinuous Galerkin Methods, designed for irregular subdomains and piecewise constant coefficients ρ aligned with the subdomain decomposition. Our results demonstrate scalability and linear dependence on H/δ, consistent with previous studies that consider triangular subdomains or continuous function spaces. This extends the applicability of our algorithm beyond studies such as [13], building upon the concept of virtual spaces analyzed in [3]. Besides a theoretical framework for analyzing the condition number of the preconditioned system, future work includes the use of adaptive algorithms like the one analyzed in [6] for high-contrast multiscale coefficients, as well as a generalization to discontinuous virtual element spaces, where $\{\mathcal{T}_h\}$ can include more general polygonal partitions of Ω.

Acknowledgments

Authors gratefully acknowledge the institutional support for Project 821-C1-228 subscribed to the Vice-Rectory for Research, University of Costa Rica.

References

[1] D. N. Arnold, F. Brezzi, B. Cockburn, L. D. Marini, *Unified analysis of discontinuous Galerkin methods for elliptic problems*. SIAM J. Numer. Anal. **39**(2001/02), no. 5, 1749–1779. DOI: 10.1137/S0036142901384162

[2] G. A. Baker, *Finite element methods for elliptic equations using nonconforming elements*. Math. Comp. **31**(1977), no. 137, 45–59. DOI: 10.2307/2005779

[3] J. G. Calvo, *On the approximation of a virtual coarse space for domain decomposition methods in two dimensions*. Math. Models Methods Appl. Sci. **28**(2018), no. 7, 1267–1289. DOI: 10.1142/S0218202518500343

[4] J. G. Calvo, *An overlapping Schwarz method for virtual element discretizations in two dimensions*. Comput. Math. Appl. **77**(2019), no. 4, 1163–1177. DOI: 10.1016/j.camwa.2018.10.043

[5] J. G. Calvo, *DGM Library*. https://github.com/jgcalvo/DGM. 2024.

[6] J. G. Calvo, J. Galvis, *Robust domain decomposition methods for high-contrast multiscale problems on irregular domains with virtual element discretizations*. Journal of Computational Physics **505**(2024), 112909. DOI: 10.1016/j.jcp.2024.112909

[7] A. Cangiani, Z. Dong, E. H. Georgoulis, *hp-version discontinuous Galerkin methods on essentially arbitrarily-shaped elements*. Math. Comp. **91**(2021), no. 333, 1–35. DOI: 10.1090/mcom/3667

[8] B. Cockburn, G. E. Karniadakis, C.-W. Shu, *Discontinuous Galerkin Methods: Theory, Computation and Applications*. 1st. Springer Publishing Company, Incorporated, 2011. DOI: 10.1007/978-3-642-59721-3

[9] D. A. Di Pietro, A. Ern, *Mathematical aspects of discontinuous Galerkin methods*. Vol. 69. Mathématiques & Applications (Berlin) [Mathematics & Applications]. Springer, Heidelberg, 2012, xviii+384. DOI: 10.1007/978-3-642-22980-0

[10] C. R. Dohrmann, O. B. Widlund, *An alternative coarse space for irregular subdomains and an overlapping Schwarz algorithm for scalar elliptic problems in the plane*. SIAM J. Numer. Anal. **50**(2012), no. 5, 2522–2537. DOI: 10.1137/110853959

[11] X. Feng, O. A. Karakashian, *Two-level additive Schwarz methods for a discontinuous Galerkin approximation of second order elliptic problems*. SIAM J. Numer. Anal. **39**(2001), no. 4, 1343–1365. DOI: 10.1137/S0036142900378480

[12] X. Feng, O. A. Karakashian, *Analysis of two-level overlapping additive Schwarz preconditioners for a discontinuous Galerkin method*. Domain decomposition methods in science and engineering (Lyon, 2000). Theory Eng. Appl. Comput. Methods. Internat. Center Numer. Methods Eng. (CIMNE), Barcelona, 2002, 237–245.

[13] O. Karakashian, C. Collins, *Two-level additive Schwarz methods for discontinuous Galerkin approximations of second-order elliptic problems*. IMA J. Numer. Anal. **37**(2017), no. 4, 1800–1830. DOI: 10.1093/imanum/drw061

[14] G. Karypis, V. Kumar, *METIS: A Software Package for Partitioning Unstructured Graphs, Partitioning Meshes, and Computing Fill-Reducing Orderings of Sparse Matrices*. Sept. 1998.

[15] B. Rivière, *Discontinuous Galerkin Methods for Solving Elliptic and Parabolic Equations: Theory and Implementation*. Frontiers in Applied Mathematics. Society for Industrial and Applied Mathematics, 2008. DOI: 10.1137/1.9780898717440

[16] A. Toselli, O. B. Widlund, *Domain Decomposition Methods-Algorithms and Theory*. Vol. 34. Springer Ser. Comput. Math. Springer, 2005. DOI: 10.1007/b137868

[17] O. B. Widlund, C. R. Dohrmann, *Small coarse spaces for overlapping Schwarz algorithms with irregular subdomains*. Domain decomposition methods in science and engineering XXIV. Vol. 125. Lect. Notes Comput. Sci. Eng. Springer, Cham, 2018, 553–560.